Paper

Application of an Acousto-optic Laser Deflector to Interferometric Measurement of Discharges in Air

Tetsuo Fukuchi* Member
Koshichi Nemoto* Member
Kouji Matsumoto** Student Member
Kiichiro Uchino*** Member

An acousto-optic laser deflector was applied to laser interferometric measurement of impulse discharges in air as a high-speed shutter. Laser interference fringes were obtained at exposure times of about 1 μs. The deflector was also used for time-resolved imaging of laser interference fringes by using a sequence of high frequency signals with different frequencies to deflect the laser beam to different angles at different times, allowing multiple interference images to be captured on a single video frame. Changes in laser interference fringes due to an impulse discharge in air showed electron densities of about 2×10^{24} m^{-3} and perturbation in the neutral density expanding at speeds of about 10^3 m/s.

Keywords: acousto-optic laser deflector, high-speed imaging, laser interferometer, discharge in air

1. Introduction

Measurement of electron and neutral density profiles in discharges and plasmas is important in fundamental science and in high voltage applications. In many cases, such as in high voltage discharges in air, the use of conductive probes is not appropriate because of their perturbative effects on the local electric field distribution. As nonperturbative diagnostic methods, optical measurement methods are commonly used. For electron density measurement, spectroscopic techniques such as spectral line emission, continuous spectrum emission, and Stark line broadening[1], as well as laser diagnostic techniques such as Thomson scattering[2] and laser interferometry[3] have been used. Laser diagnostic techniques are preferable because of their good spatial and temporal resolution. Moreover, emission spectroscopy generally requires assumptions of local thermal equilibrium or excitation models, and Stark line broadening is difficult to isolate from Doppler and collisional broadening[1], which is the case in atmospheric discharges with low ionization. When Thomson scattering and laser interferometry are compared, the latter is better suited for measurement of electron density distribution in atmospheric discharges, since Thomson scattering is generally limited to one spatial location, and care must be paid to eliminate stray laser light and scattering by air molecules and particles, since the signals are very weak.

Of the various laser interferometers that are available, Mach-Zender interferometers have been most commonly used for discharge measurement[3]~[5]. Pulsed lasers, such as nitrogen and ruby lasers[3], excimer pumped dye lasers[4], and Nd:YAG lasers[5] have been used. In these experiments, the interference patterns were obtained at a fixed time delay relative to the discharge.

In the case of transient discharges in which the spatial and/or temporal reproducibility is poor, measurement of the variation of interference fringes (time-resolved imaging) for a single discharge is desirable. Since the repetition rate of pulsed lasers is generally in the order of Hz or kHz, where as a typical impulse discharge occurs in the order of μs, the use of pulsed lasers for time-resolved imaging is difficult. An alternative method is the use of a continuous wave (cw) laser and a high-speed imaging device to capture the laser interference fringes with frame rates of 10^6 frames/s or more. Commonly, an ultra high-speed framing camera incorporating an image intensifier, which is commercially available, is used for these applications. However, this type of camera is very costly, and there is danger of damaging the image intensifier when the incident light is of high intensity, which is the case of detecting laser interference fringes. Therefore, a low-cost, robust high-speed shutter, which can be used with an ordinary CCD camera, is desired. Electronic shutters on ordinary CCD cameras have top speeds of 10-100 μs and are insufficient for capturing changes in the interference fringe pattern, which occur in the order of μs or less.

2. Acousto-optic Laser Deflector

In this study, an acousto-optic (AO) laser deflector, which can change the direction of the incident laser beam at high-speed, was used as a shutter to perform high-speed imaging and time-resolved imaging of laser interference fringes. The principle of using an AO laser deflector as a shutter has been previously demonstrated[6].

2.1 Operation Principle A schematic diagram of an AO laser deflector is shown in Fig. 1[7]. When a high frequency signal is applied to an AO crystal via an acoustic transducer, incident light is diffracted by the acoustic waves which propagate through the crystal. The diffraction angle θ is given by $\theta=f\lambda/V$, where λ is the wavelength of the incident light, f is the acoustic wave frequency, and V is the acoustic wave speed. The diffraction

* Electrical Physics Department, Komae Research Laboratory, Central Research Institute of Electric Power Industry
2-11-1 Iwado-kita, Komae 201-8511
** Graduate School of Engineering, Kanagawa University
3-17-1 Rokkakubashi, Kanagawa-ku, Yokohama 221-8686
*** Interdisciplinary Graduate School of Engineering Sciences, Kyushu University
6-1 Kasuga Koen, Kasuga-shi, Fukuoka 816-8580

efficiency, which represents the proportion of the diffracted light power to the incident light power, is given by $\eta=\sin^2[(\pi/\lambda)(MPL/2H)^{1/2}]$, where M is the figure of merit which depends on the material, P is the input power of the high frequency signal, and LxH is the geometrical dimension of the cross section of the crystal perpendicular to the direction of propagation of the acoustic wave. Commonly used AO materials are Ge, GaP, InP, $LiNbO_3$, TeO_2, SiO_2 [7].

2.2 Specifications In this study, an AO laser deflector (Brimrose, TED5-80-50-.532-AR) using TeO_2 as the substrate was used. TeO_2 was chosen because the acoustic wave speed (V=660 m/s, slow shear mode) is very low and thus large diffraction angles can be obtained. When the deflector is used as a shutter, the undiffracted light must be entirely blocked, so a large angular discrimination, or angular separation between the undiffracted and diffracted beams, is preferable. The acoustic wave frequency response is centered at f=80 MHz with a bandwidth of 55 MHz. For an incident wavelength of 532 nm, the center frequency corresponds to a diffraction angle of 3.7 degrees. The transmission of the crystal is >95%, and the wavefront distortion is $<\lambda/10$. Since most of the optical elements used in a typical laser interferometer have surface flatness of $\lambda/10$, the distortion due to the laser deflector can be neglected. The input power is <1W, and the optimal input power is 0.28 W, which results in a maximum diffraction efficiency of η=75%. The AO crystal is housed in a metallic case of length 34 mm, width 45 mm, and height 23 mm. There are windows of 10x5 mm on opposite lengthwise sides of the metallic case for laser beam input and output. The crystal can accommodate a maximum laser beam diameter of 3 mm.

The high frequency signal source, or AO driver, can generate pulses of frequencies 68, 76, 84, 92 MHz. For use as a fast shutter, as described in Section 3, a single frequency is used. In time-resolved imaging, as described in Section 4, all four frequencies are used to obtain four images at different times. The accuracy of each frequency is 0.015%, and the modulation frequency response is DC-10 MHz. Therefore, a minimum gate width of 100 ns is possible.

2.3 Temporal Response Since the laser deflector diffracts the incident light by acoustic waves propagating through the crystal, there is a time delay from the application of the high frequency signal until the diffraction takes place. This is mainly due to the time required for the acoustic wave to propagate from the crystal-transducer interface to the location of the incident laser spot[6]. A typical time response of the AO laser deflector is shown in Fig. 2. In this measurement, diffracted light was monitored by a photomultiplier tube (PMT) positioned to detect only the diffracted light. The upper trace in Fig. 2 shows the gate signal input to the high frequency signal source, and the lower trace shows the PMT output. There is a time delay of 0.87 μs from the rise of the gate to the PMT signal peak. The PMT signal shows a full width at half maximum (in absolute value) of 1.12 μs, which is close to the width of the gate input pulse, which was set to 1.1 μs. The shot-to-shot fluctuation of the time delay between the gate signal and PMT signal was negligible, and can be considered to be below 10 ns.

2.4 Application to a Laser Interferometer The AO laser deflector was applied to a Mach-Zender laser interferometer, as shown in Fig. 3. The beam from a diode-pumped, cw, single-mode Nd:YAG laser of wavelength 532 nm and output power 5 mW (CrystaLaser, GCL-005-SLM) was expanded to a

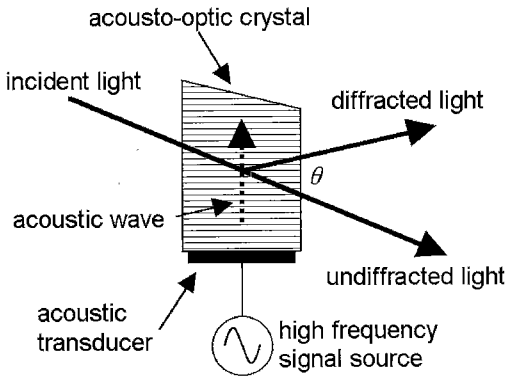

Fig. 1. Schematic diagram of an acousto-optic laser deflector

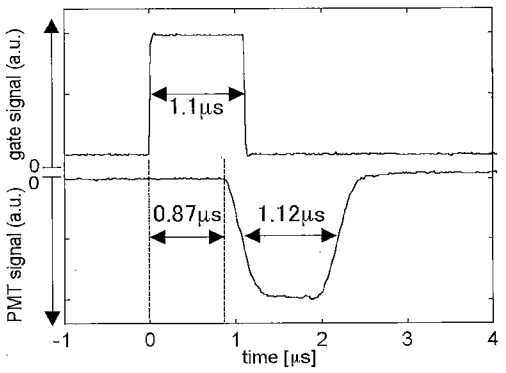

Fig. 2. Time response of the acousto-optic laser deflector

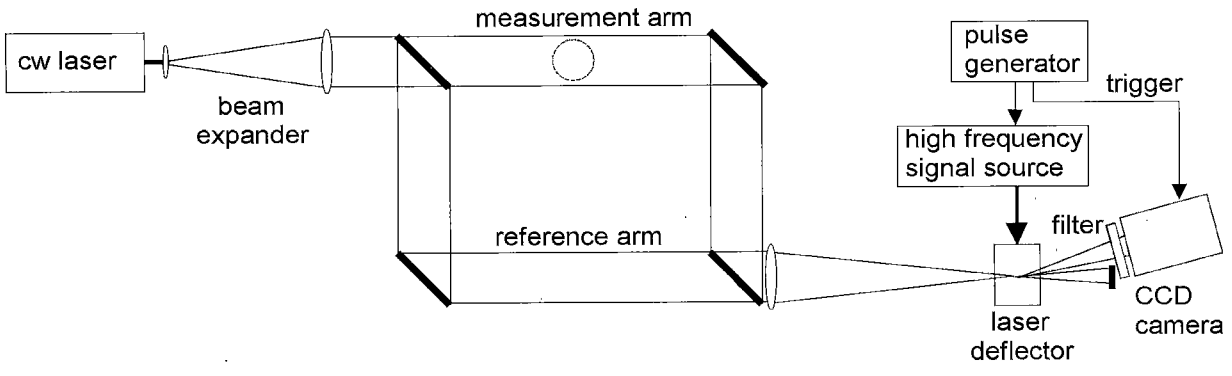

Fig. 3. Schematic of the Mach-Zender laser interferometer incorporating the acousto-optic laser deflector as a shutter

beam diameter of 30 mm by a beam expander consisting of a 40× microscope objective lens and a plano-convex lens of focal length 500 mm, and split into reference and probe beams by a 1:1 broadband beamsplitter. The probe beam was passed through the discharge region, the two beams were combined by a second beamsplitter, and the resultant beam, which carries the laser interference pattern, was reduced to a diameter of 2-3 mm at the entrance of the AO laser deflector by a plano- convex lens of focal length 300 mm. The optical path length between the two beamsplitters was 1.55 m. The diffracted beam from the AO deflector was directed to a CCD camera (NEC, TI-150V) while the undiffracted beam was blocked in front of the camera. In order to prevent the strong optical emission of the discharge from entering the camera, an interference filter of center wavelength 532 nm and bandwidth 0.8 nm was placed in front of the CCD camera. The CCD camera shutter can be triggered externally, and can function at video rate with the shutter speed set to 1/30 s. However, since the temporal region of interest in discharge diagnostics is in the order of μs, the shutter speed was set to 1 ms in order to reduce the noise due to background light which passes through the interference filter. The CCD camera is of 1/2-inch format with 648×485 effective pixels, with an intensity resolution of 8 bits (256 colors) grayscale. The video output consists of 640 ×480 pixels.

3. Application to Measurement of Impulse Discharges in Air

The laser interferometer described in Section 2.4 was used to detect temporal and spatial changes in the laser interference fringes which result from optical path differences arising from impulse discharges in air.

3.1 Experimental Configuration A schematic diagram of the experimental apparatus used for discharge measurement is shown in Fig. 4. An impulse voltage generator (Pulse Electronic Engineering, IVG-200A) of maximum charging voltage 200 kV generated an impulse voltage of negative polarity, risetime 1.2 μs, falltime 50 μs, and maximum voltage ~90kV (measured without load). In order to minimize time jitter of the discharge, the impulse generator was triggered by focusing a pulse from a Q-switched Nd:YAG laser (Spectra-Physics, GCR190) on the initial sphere-sphere gap. The observed time jitter was <30 ns for a sequence of 30 shots. The impulse voltage was applied to the needle electrode of a needle-needle or needle-rod electrode gap, typically of gap length 10-20 mm. Since the maximum voltage of the impulse voltage was about twice the sparkover voltage of the electrode gap, the voltage was truncated before reaching the maximum value. The applied voltage was monitored by a voltage divider of ratio 18,300:1, and the current on the ground electrode side was monitored by a Rogowski coil (Pearson, 411) of sensitivity 0.1 V/A. Typical voltage and current waveforms for a gap length of 17 mm are shown in Fig. 5. In this case, the sparkover voltage of the electrode gap was about −40 kV.

A logic signal concurrent with flashlamp firing of the GCR190 laser was used to trigger a delay generator (Stanford Research, DG535), which provided the gate signals to the high frequency signal source and the trigger signal for the CCD camera shutter. Since the flashlamp excitation occurs 200 μs before the Q-switched pulse (which triggers the impulse generator), the laser interference fringes can be imaged before the impulse discharge.

The AO laser deflector and CCD camera were arranged so that interference fringes corresponding to a region of about 20 mm in height (in the direction of the electrode gap) and 10 mm in width (in the direction perpendicular to the electrode gap, centered on the high voltage needle electrode) were obtained. The spatial scale of the CCD camera output was calibrated by placing apertures of known size in the electrode gap region and monitoring the spot size of the images.

3.2 Measurement Results The laser interference fringes obtained using a gate width of 1 μs are shown in Fig. 6. Images A-H show the interference fringes obtained at t=-0.3, 0.0, 0.5, 1.0, 1.5, 2.0, 2.5, 3.0 μs relative to sparkover, respectively. The shadow of the high voltage needle electrode can be seen at the top center of each image. Each image corresponds to a spatial dimension of height 17 mm and width 8.5 mm at the discharge region, and the spacing between successive fringes corresponds to approximately 1 mm. Since images A-H were obtained for different discharge shots, variation in the path of the discharge is seen.

In Fig. 6B-C, a vertical streak emerging from the tip of the needle electrode can be seen, but the shift in the interference fringes cannot be detected along its path. This may be because the perturbations are below the sensitivity limit. In Fig. 6D-H, the downward shift in the interference fringes, which is a result of the increase in electron density and decrease in neutral gas density in the discharge, can be clearly seen. In Fig. 6H, a slight upward shift in the fringes in the outer region is also seen. This represents an

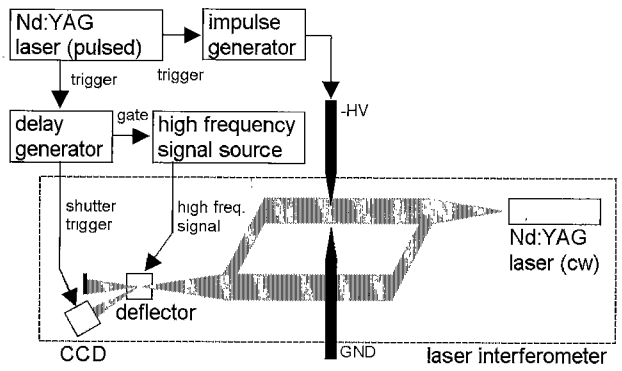

Fig. 4. Schematic diagram of the experimental configuration

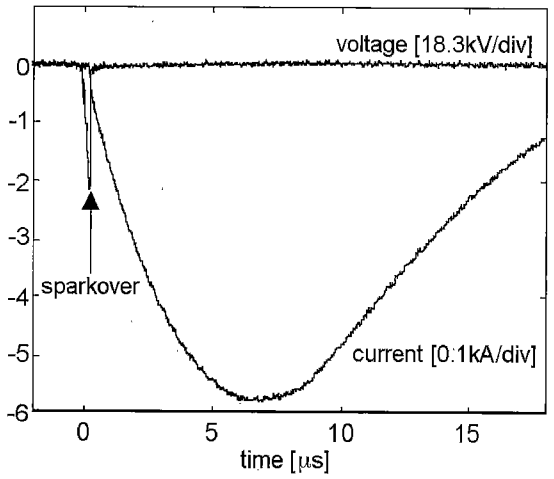

Fig. 5. Typical voltage and current waveforms of the impulse discharge in air

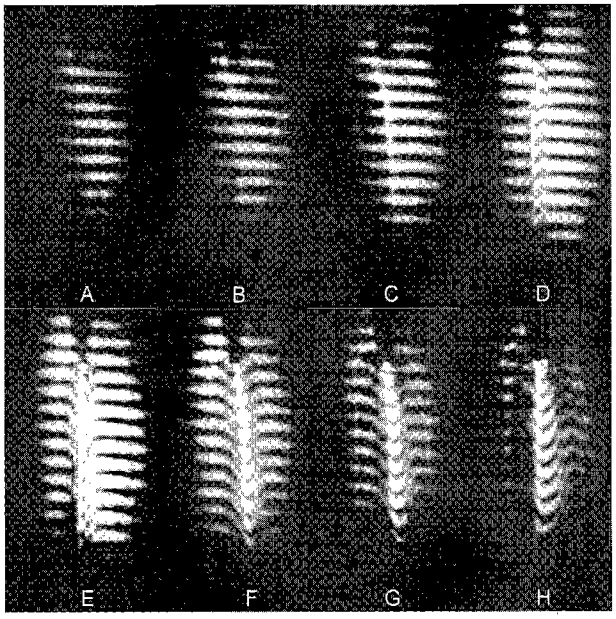

Fig. 6. Variation in laser interference fringes due to impulse discharge in air (A-H: exposure starting at -0.3, 0.0, 0.5, 1.0, 1.5, 2.0, 2.5, 3.0 μs relative to sparkover, gate duration 1.0 μs)

increase in the neutral gas density, which suggests the presence of a shock front.

The electron density N_e can be estimated using the changes in the interference fringes obtained in the early stages of the discharge, in which the neutral gas molecules can be considered to be stationary and the fringe shift ΔF can be considered to be solely due to N_e. The optical path difference at wavelength λ due to an electron density of N_e is given by

$$\Delta L = \left(-e^2\lambda^2 / 8\pi^2 c^2 m_e \varepsilon_o\right) N_e L = \left(-4.47\times10^{-16} m\right)\lambda^2 N_e L \quad \cdots\cdots (1)$$

where L is the spatial extent of the plasma[8]. Since $\Delta F = \Delta L/\lambda$, a shift of 1 fringe ($\Delta F$=1) at λ=532 nm corresponds to an line-integrated electron density of N_eL=4.4×10^{21} m^{-2}. In Fig. 6D-E, the fringe shift is about ΔF=0.5－0.8 and the plasma column width is about L=1 mm, which results in an electron density of N_e=(2.1－2.7)×10^{24} m^{-3}. This is in rough agreement with the electron densities previously obtained for an atmospheric impulse arc[2][3], although a direct comparison cannot be made because of the difference in discharge characteristics.

The expansion speed of the neutral density perturbation can be estimated from the movement of the outer perimeter of the perturbed region in Fig. 6F-H. The rate of expansion is about (2 mm)/(1 μs)=2×10^3 m/s, so the propagation speed in each direction is estimated to be 10^3 m/s, or about 3 times the speed of sound in unperturbed air.

4. Time-resolved Imaging of Inter- Ference Fringes

The use of the AO laser deflector as a fast shutter was shown in Section 3. However, due to spatial fluctuations in the discharge, it is desirable to obtain changes in the laser interference fringes for a single discharge, which requires time-resolved imaging. In this section, the application of the AO laser deflector to time-resolved imaging is presented.

4.1 Operation Principle Since the AO laser deflector

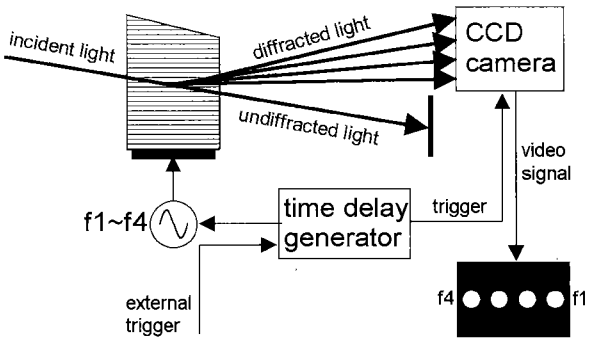

Fig. 7. Schematic diagram of time-resolved imaging using the AO laser deflector

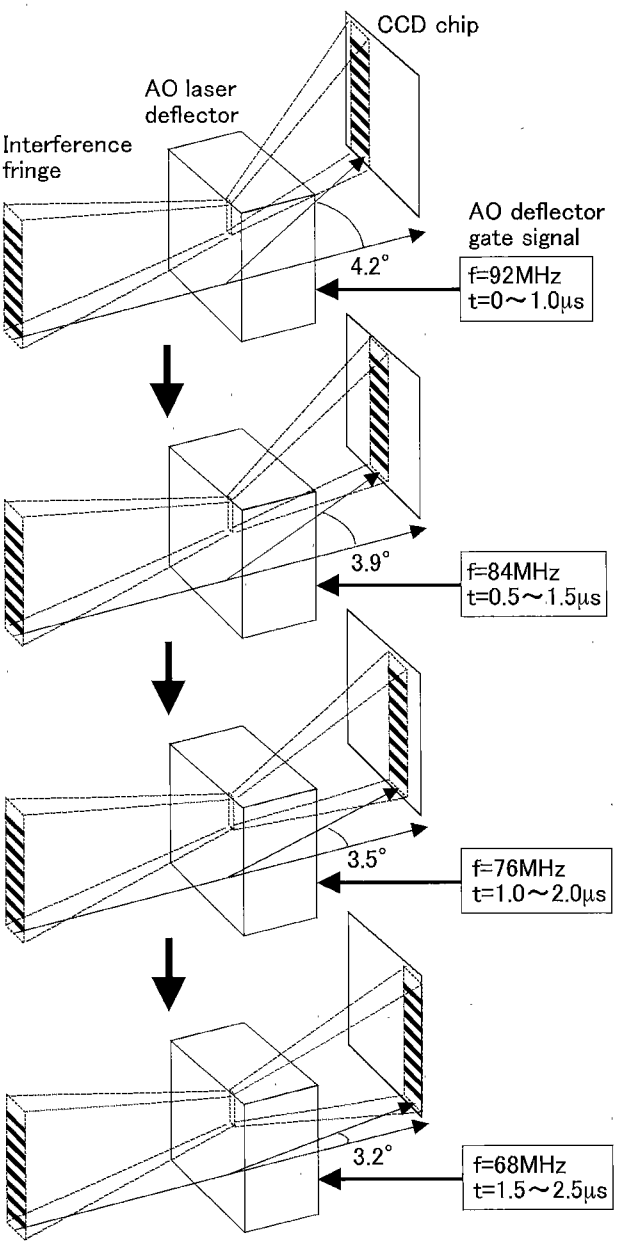

Fig. 8. Schematic diagram of time-resolved imaging of laser interference fringes, in which successive application of high frequency pulses result in different diffraction angles at different times (size and angles are not drawn to scale)

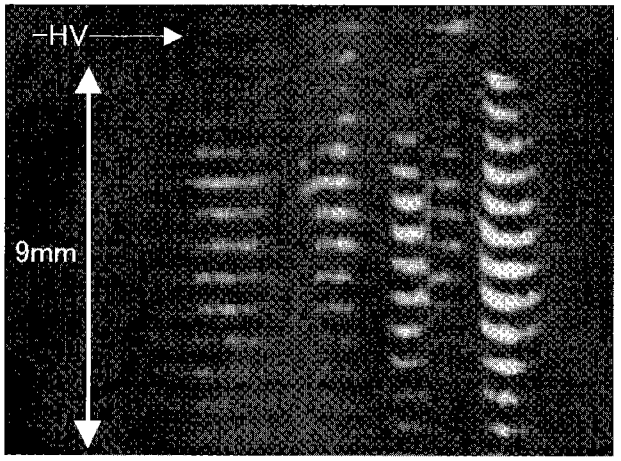

Fig. 9. Example of time-resolved imaging of laser interference fringes with time separation 0.5 μs and gate width 1.0 μs

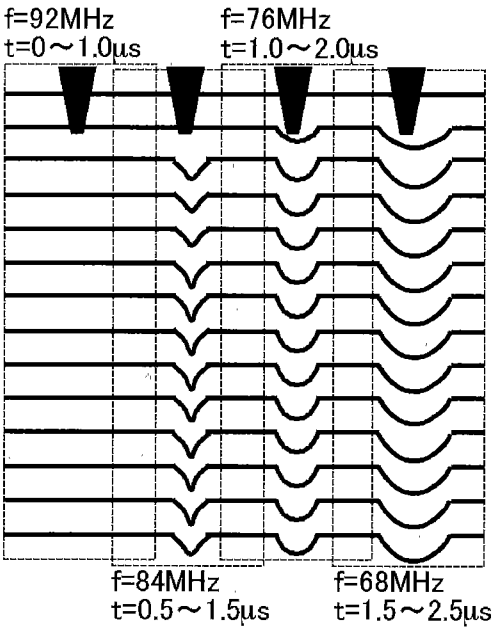

Fig. 10. Schematic diagram indicating the regions of the four frames of laser interference fringes shown in Fig. 9

operates at a center frequency of 80 MHz and a bandwidth of 55 MHz, it is possible to apply high frequency pulses of different frequency and change the diffraction angle as a function of time. This results in projection of the laser beam (corresponding to different times) on different regions of the CCD chip, allowing multiple spots to be imaged on a single video frame. A schematic diagram of time-resolved imaging using the AO laser deflector is shown in Fig. 7. When high frequency signals of frequencies f_1, f_2, f_3, f_4 ($f_1<f_2<f_3<f_4$) are applied sequentially, the diffracted light emerges from the deflector at four different angles. The CCD camera is positioned so that all spots impinge on the CCD chip. In this configuration, the diffraction angle corresponding to f_4 is largest, so the spot appears on the left side of the screen. For convenience, to order the spots in temporal order from left to right, the temporal order of application of the pulses is f_4, f_3, f_2, f_1. The timing and pulse width of each frequency can be arbitrarily adjusted, so the exposure time and duration can be adjusted, as long as all pulses lie within the exposure time of the CCD camera shutter.

A schematic diagram of time-resolved measurement of laser interference fringes is shown in Fig. 8. High frequency signals of frequencies f_4=92 MHz, f_3=84 MHz, f_2=76 MHz, f_1=68 MHz were applied in a burst mode, which resulted in deflection angles of 4.2, 3.9, 3.5, and 3.2 degrees, respectively (the beam size and angles in Fig. 8 are not drawn to scale). The pulse duration was set to 1 μs and the pulse separation was set to 0.5 μs. The application of different frequencies resulted in imaging of the laser interference fringe on different regions of the CCD chip, representing high-speed imaging of four frames with an exposure time of about 1 μs and an inter-frame spacing of 0.5 μs, or a frame rate of 2×10^6 frames/s. As shown in Fig. 8, the incident light was focused at the location of the AO laser deflector, so the diffracted beam expanded. The CCD camera was placed so that the height of the diffracted beam matched the vertical dimension of the CCD chip.

4.2 Measurement Results An example of time-resolved imaging of laser interference fringes using the experimental configuration shown in Fig. 4 is shown in Fig. 9. The four frames captured are shown schematically in Fig. 10. Since the angular separation between successive images is smaller than the angular size of each frame, the outer parts of the interference fringes have overlapped, resulting in an appearance of a single image. Figure 9 represents the CCD camera video output of 640x480 pixels. The distance from the tip of the high voltage electrode (labeled as -HV), whose shadow is visible at the upper end, to the lower end of the image is 9 mm. Expansion of the discharge region is clearly visible, with a rate of expansion of about (0.6 mm)/(0.5 μs)=1.2×10^3 m/s. Since the outer perimeter of the perturbed region was not clearly visible, the expansion speed of the neutral density perturbation could not be determined.

5. Conclusion

In summary, an acousto-optic laser deflector was applied to laser interferometric measurement of discharges in air as a high-speed shutter for imaging of laser interference fringes. Time-resolved imaging of laser interference fringes at a frame rate of 2×10^6 frames/s was also demonstrated.

Although the laser interferometer was specifically applied to discharge diagnostics, this method can also be used for other applications requiring high-speed imaging, such as combustion diagnostics, ultrasound applications, and material destruction studies.

Acknowledgement

The authors would like to express their gratitude to Dr. Shirabe Akita of the Central Research Institute of Electric Power Industry for helpful discussion and advice.

(Manuscript received April 15, 2003, revised July 30, 2003)

References

(1) H Griem : Plasma Spectroscopy, Mc-Graw Hill, New York (1964)

(2) K. Uchino, K. Muraoka, and M. Akazaki : "Studies of an Atmospheric Impulse Arc by Ruby-Laser Scattering", *T. IEE Japan*, Vol. 103-A, No 11, pp. 609-616 (1983-11) (in Japanese)

(3) M. Akazaki, K. Muraoka, and M. Hamamoto : "Studies of an Atmospheric Impulse Arc Using a Two-Wavelength Laser Interferometry", *T. IEE Japan*, Vol. 101-A, No 5, pp. 255-262 (1981-5) (in Japanese)

(4) T Ikegami, H. Arakaki, K. Ebihara, M. Akazaki : "Optical Measurement of Breakdown Plasma Generated by Laser", *T. IEE Japan*, Vol. 115-A, No. 7, pp. 637-643 (1995-7) (in Japanese)

(5) W D. Kimura, M. J. Kushner, E. A. Crawford, and S. R. Byron : "Laser Interferometric Measurements of a Laser-Preionization- Triggered Spark Column", *IEEE Trans. Plasma Sci.*, Vol. PS-14, No. 3, pp. 246-255 (1986-6)
(6) T. Fukuchi, T Nayuki, K. Nemoto, and K. Uchino . "Development of a high-speed laser interferometer using an acousto-optic deflector", *IEEJ Trans. EIS*, Vol. 123-C, No 9 , pp 1531-1536 (2003-9) (in Japanese)
(7) Acousto-Optic Modulators, Brimrose Corp. of America, Baltimore (1996)
(8) K. Muraoka and M. Maeda : Applied Laser Diagnostics for Gases and Plasmas, Sangyo Tosho, Tokyo (1995) (in Japanese)

Tetsuo Fukuchi (Member) was born in 1962. In Aug. 1995 he received the Ph.D. degree in physics from the University of California, Los Angeles, USA. In Feb. 1996 he joined the Central Research Institute of Electric Power Industry. He is engaged in development of laser diagnostic techniques of discharge phenomena, development of optical and laser techniques for leak gas and trace gas detection. He is currently a member of the Japan Society of Applied Physics.

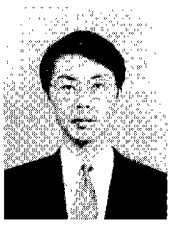

Koshichi Nemoto (Member) was born in 1959. In Mar. 1984 he received the M.S. degree in electrical engineering from the University of Tokyo, Tokyo, Japan. In Apr. 1984 he joined the Central Research Institute of Electric Power Industry. From Dec. 1989 to Jul. 1993, he was a researcher at the Laser Atomic Separation Engineering Research Association of Japan. In Mar. 1998 he received the D.Eng. degree in electrical engineering from the University of Tokyo. From Oct. 1998 to Dec. 1999, he was a visiting scientist at the Center for Ultrafast Optical Science of the University of Michigan, USA. He is engaged in development of lasers, development of laser intensity distribution control techniques, high intensity laser research. He is currently a member of the Japan Society of Applied Physics and the Laser Society of Japan.

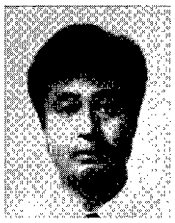

Kouji Matsumoto (Student Member) was born in 1981. In Mar. 2003 he received the B.S. degree in electrical engineering from Kanagawa University. In Apr. 2003 he entered the M.S. program at Kanagawa University, where he is presently a graduate student. He is enganged in development of laser diagnostic techniques of discharge phenomena.

Kiichiro Uchino (Member) was born in 1955. In Mar. 1983 he received the D.Eng. degree from Kyushu University, Fukuoka, Japan. In Apr. 1983 he joined Kyushu University as a research assistant, in Apr. 1986 he became associate professor, and in Apr. 1998 he became professor. He is engaged in laser diagnostics and applications of discharge plasmas. He is currently a member of the Japan Society of Applied Physics, the Japan Society of Physics, the Plasma and Fusion Society, and the Laser Society of Japan.

◇ ◇ ◇

◇ ◇ ◇